

Barrier tuning of atomic layer deposited Ta₂O₅ and Al₂O₃ in double dielectric diodes

Running title: Barrier tuning of Ta₂O₅ and Al₂O₃ in resonant tunneling diodes

Running Authors: Nemr Nouredine et al.

Ibrahim Nemr Nouredine

Naser Sedghi

Ivona Z. Mitrovic

Steve Hall^{a)}

University of Liverpool, Department of Electrical Engineering and Electronics, Brownlow Hill, L69 3GJ Liverpool, UK

^{a)} Electronic mail: s.hall@liv.ac.uk

The performance of ultra-thin atomic layer deposited dielectrics of low (Al₂O₃) and high (Ta₂O₅) electron affinity (χ) is investigated in metal-insulator-(insulator)-metal, or *MI(IM)*, diodes. The conduction mechanisms in 4 nm thick atomic layer deposited Al₂O₃ and Ta₂O₅ single barrier *MIM* diodes are first studied to show the dominance of tunneling and thermally activated Poole-Frenkel emission respectively in these oxides. Varying the layer thickness of Ta₂O₅ with a 1 nm thick layer of Al₂O₃, shows evidence for resonant tunneling in double barrier *MIM* structures and is correlated with the simulated bound states in the quantum well formed between the two dielectrics. These findings demonstrate experimental work on barrier tuning of resonant tunneling diodes with sufficient rectifying capability at a turn-on voltage as low as 0.32 V enabling their potential use in terahertz applications.

I. INTRODUCTION

Diodes based on tunneling through one or more insulator layers are attractive rectifying devices for electronics and energy harvesting applications at terahertz (THz) and infrared (*IR*) frequencies¹, offering rectification into these regimes due to their short tunneling transit time in the range of femtoseconds². Due to their ultrafast operation, these diodes are of interest for optical frequency applications^{3,4} including infrared detection^{5,6} and solar energy harvesting^{7,8}. Integrating them into rectenna arrays⁹ offer the distinct advantage over photovoltaics of harvesting *IR* energy during night time hours. The main challenges remain in achieving sufficient non-linearity, high asymmetry and low dynamic resistance¹⁰ to achieve sufficiently high efficiency. Resonant tunneling (*RT*) can serve to bring further enhancement to the current asymmetry and non-linearity¹¹ with demonstrated operation at THz frequencies^{12,13}.

The device structure comprises of one or two dielectric layers of a few nanometer thickness sandwiched between two metal electrodes. The aim is to develop diodes with sufficiently non-linear and asymmetric current density-voltage (*J-V*) characteristics which can be achieved by the choice of the dielectrics and their thicknesses. Asymmetry is defined as the ratio of the current (*I*) at positive bias to that at negative bias at certain voltage $f_{asym} = I_+/I_-$. The dynamic resistance is defined as $R_d = dV/dI$. Non-linearity is defined as the ratio of the static to dynamic resistance $f_{NL} = (V/I)/R_d$,¹⁴ and needs to be greater than about three¹⁵.

In this contribution, the conduction mechanisms dominating in 4 nm thick atomic layer deposited (*ALD*) Al_2O_3 and Ta_2O_5 are studied in *MIM* structures. With 1 nm of the

former and 1 to 4 nm thickness tuning of the latter, the effect of *RT* on *MIIM* diode performance is investigated experimentally by studying the effect of varying the thickness of one layer in an *MIIM* structure.

II. FABRICATION

Devices with lateral area of $100 \times 100 \mu\text{m}^2$ of structures presented in *Table I* were fabricated on cleaned Corning glass substrates. The top and bottom metal layers of 50 nm thickness were deposited by thermal evaporation through a shadow mask. The Al_2O_3 and Ta_2O_5 oxides were successively deposited over the bottom electrodes by *ALD* at a temperature of 200 °C using deionized water as the oxidant for Ta_2O_5 and Al_2O_3 at 0.04s/10s pulse/purge time, tantalum ethoxide precursor for Ta_2O_5 at 0.3s/2s pulse/purge time, and trimethylaluminium (*TMA*) precursor for Al_2O_3 at 0.02s/5s pulse/purge time. The thicknesses of the dielectric layers were measured by variable angle spectroscopic ellipsometry using a *XLS-100 J.A. Woollam* instrument. The *J-V* measurements were done in the dark using an *Agilent B1500 Semiconductor Device Analyzer* on a temperature controlled heating stage. Voltage was swept from 0 V with 10 mV step size in negative and positive bias.

Table I. Device structure and layer thickness.

	Bottom	Al_2O_3	Ta_2O_5	Top
	Thickness [nm]			
S1	Au	4	-	Al
S2	Al	-	4	Al
S3	Cr	1	1	Al
S4	Cr	1	2	Al
S5	Cr	1	3	Al
S6	Cr	1	4	Al

III. Material Selection

The possible tunneling mechanisms in each structure are illustrated schematically using the energy band diagrams shown in *FIG. 1* considering literature values for the work functions (4.2¹⁶, 4.4¹⁶, and 5.1¹⁷ eV for Al, Cr, and Au respectively) and electron affinity, $q\chi$ ¹⁸, of 1.35 and 3.75 eV for Al₂O₃ and Ta₂O₅, respectively. These values and a dielectric constant of 10¹⁹ and 25²⁰, for Al₂O₃ and Ta₂O₅, respectively, have been used for all theoretical calculations. When electrons are injected from the bottom electrode (right to left on the diagrams) at negative bias, the current in single barrier structures could be driven by direct or Fowler-Nordheim (*FN*)²¹ tunneling; the latter is depicted for the case of S2 in *FIG. 1*. For double dielectric structures, this could turn into one-barrier step tunneling²² at sufficient negative bias as for S6 and S3. For opposite injection of electrons at positive bias, *RT* may occur in double barrier *MIIM* structures when the quantum well formed between the dielectrics becomes wide and deep enough to allow the formation of bound states²³ enabling resonant tunneling. It is shown in *FIG. 1.b* that these could be achieved for S6 but not S3. Al₂O₃ has a large conduction band offset with Ta₂O₅, necessary to create the quantum well, which gets wider and deeper when it is thin enough (1 nm) and when Ta₂O₅ is thick enough (4 nm).

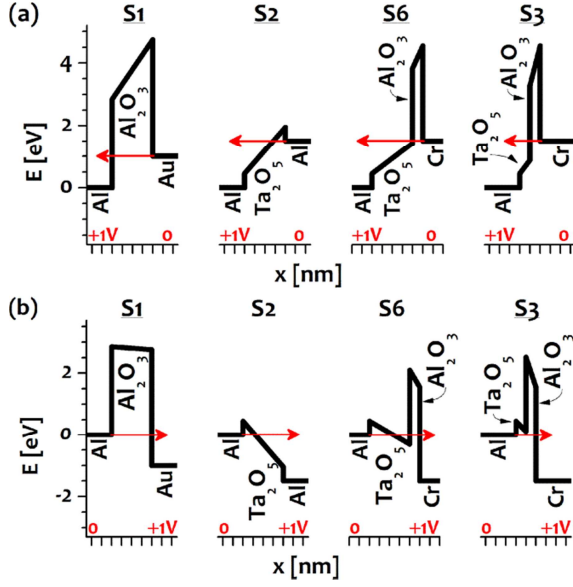


FIG. 1. Energy band diagrams (conduction band) of 4 structures at -1 (a) and $+1$ V (b). Direction of electron injection is indicated by red arrows.

Despite the advantage of Al work function to create a deep quantum well for RT at lower voltage, the AFM images of *Fig.2* reveal a large surface roughness of 2.8 nm, which is not smooth enough for deposition of such thin dielectric layers. The metals Cr and Au serve better as bottom electrodes due to their ultra-smooth surface roughness of 0.42 and 0.44 nm root mean squared (*RMS*) and their lower z -excursion peaks of 4.7 and 4.6 nm, respectively, which is necessary to avoid field intensification. These metals also have high melting point as compared to the bottom Al where the ALD growth of the oxides at 200 °C on top of it might result in the formation of interfacial layer. In addition, a few nanometer thick native oxide layer growing on top of Al when exposed to air²⁴ is undesired. Despite its low surface roughness, using Au with its large work function as a bottom electrode in *MIIM* devices increases the metal-oxide energy barrier lowering the Fermi level of the emitter electrode so that no bound states in the quantum well could be formed in the 1.5 V voltage range. The metal Cr has a work function close to that of Al

and has a native oxide of very small bandgap which does not create a large conduction band offset with Ta_2O_5 as Al. It is thus chosen as the bottom electrode for resonant tunneling structures having the advantage of its ultra-smooth surface and the possibility of forming bound states in the quantum well within the applied voltage range when used in S6 structure (FIG. 1.b). Using a few nanometer thick Ta_2O_5 of large electron affinity (3.75 eV) and of large band offset with a 1 nanometer thick Al_2O_3 (2.4 eV) allows the quantum well to be tuned below the Fermi level of the emitting electrode with the applied bias.

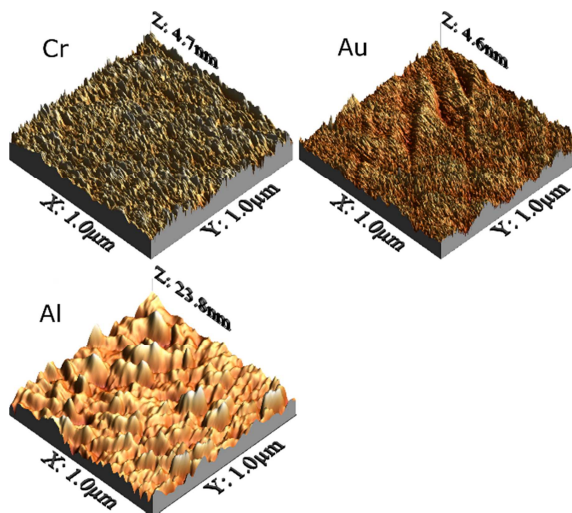


FIG 2. AFM images scanned at $1 \times 1 \mu\text{m}^2$ regions of the as-deposited bottom layers Cr, Au, and Al revealing an *RMS* average surface roughness of 0.42, 0.44, and 2.8 nm.

IV. RESULTS AND DISCUSSION

A. Conduction mechanisms in the individual dielectrics

The possible presence of thermally activated mechanisms is first studied individually in the single barrier structures of Al_2O_3 and Ta_2O_5 . The J - V characteristics show temperature insensitivity for S1 (FIG. 3.a) and strong temperature dependence for sample S2 (FIG. 3.b). This indicates that the 4 nm thick Al_2O_3 and Ta_2O_5 are dominated by tunneling and a thermal emission process, respectively, which is consistent with another study²⁵ done on 10 nm thick Al_2O_3 and Ta_2O_5 . The presence of thermally activated mechanisms Schottky emission (SE) and Poole-Frenkel emission (PFE) in S2 can be examined using the logarithmic plots of I/T^2 and I/V versus $V^{1/2}$ (FIG. 4) which showed good linear fits with respect to their corresponding governing equations²⁶ $I_{SE} \propto T^2 \exp(\frac{AV^{1/2}}{kT} - B)$ and $I_{PFE} \propto V \exp(\frac{AV^{1/2}}{kT} - B)$ respectively where A and B are constants, with a regression coefficient $R^2 > 0.995$ over the same voltage range at both polarities.

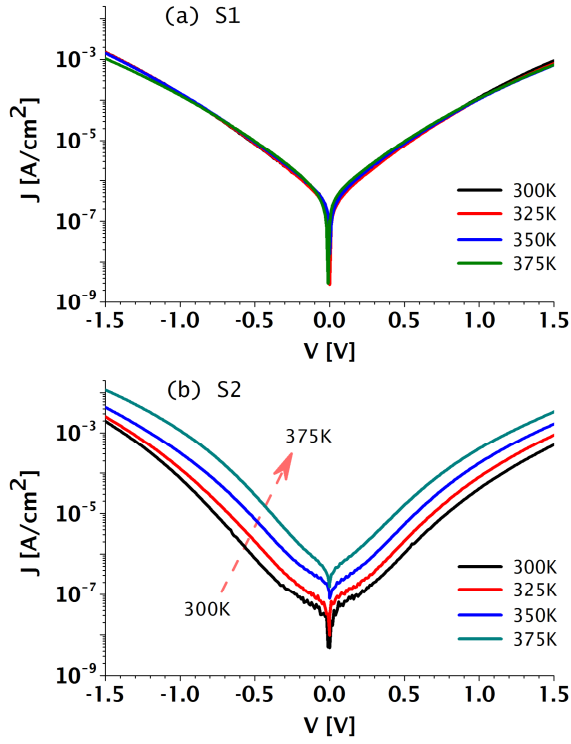


FIG. 3. J - V characteristics of the MIM devices S1 (Al_2O_3) and S2 (Ta_2O_5), measured at 300, 325, 350, and 375 K.

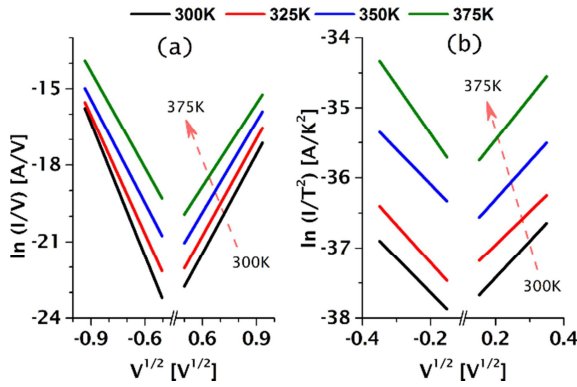


FIG. 4. PFE (a) and SE (b) plots of the MIM device S2 (Ta_2O_5) at 300, 325, 350, and 375 K.

The average optical relative permittivity $\epsilon_{r,opt}$, assumed to be equal to the square of the optical index of refraction n , of 50 nm thick ALD deposited Ta_2O_5 and Al_2O_3 on silicon

substrates was found to be 3.14 and 5.23, respectively, as extracted from the spectroscopic ellipsometry measurements at room temperature in the 400-1200 nm wavelength range. The equivalent dynamic relative permittivity ϵ_r of the 4 nm thick Ta₂O₅ extracted from the slopes of the *SE* plots (*FIG. 4.b*) at 300 K in the 0.02-0.12 V voltage range were far larger than the optical values, and thus *SE* will be ruled out for this structure (S2). Only ϵ_r extracted from *PFE* plots for S2 was self-consistent with $\epsilon_{r,opt}$ using a trap compensation factor²⁷ (*CF*) multiplied by kT in *PFE* equation ranging^{28,29} from 1 to 2. This indicates the dominance of *PFE* in the 4 nm thick Ta₂O₅ ranging widely from 0.25 to 1.5 V at both polarities (*Table II*).

Despite the work function dissimilarity of 0.9 eV¹⁶ in S1, no noticeable asymmetry could be observed due to the large barrier across the low- χ Al₂O₃ preventing the occurrence of *FN* tunneling within the applied voltage range (*FIG. 1*).

Table II. Extracted *CF* when $\epsilon_{r,PFE}$ is matched to $\epsilon_{r,opt}$ (CF_m), the voltage range in which *PFE* fitting is done (V_{PFE}), and the trap depth at zero bias ϕ_{t0} for the 4 nm thick Ta₂O₅ at negative (–) and positive (+) polarities at 300 K.

Bias	CF_m	V_{PFE} [V]	$q\phi_{t0}$ [eV]
–	1.35	0.25-1.5	0.9
+	1.81		0.53

The linear fit of the Arrhenius plots (*FIG. 5*) is used to extract the activation energy (E_a) (*FIG. 6*) associated with the dominant oxide trap in S2, such that $I_{PFE} \propto V \exp(\frac{-q}{kT} E_a)$ where k is the Boltzmann constant and T is the temperature in K. The

average trap depth at zero bias ϕ_{t0} extracted at positive bias for the 4 nm thick *ALD* Ta₂O₅ (Table II) was close to the 0.58 eV extracted for 10 nm thick *ALD* Ta₂O₅ in other studies^{25,30}. PFE is a bulk limited process and should ideally be independent of voltage polarity. The polarity dependence apparent in FIG. 3.b therefore, could be related to the difference in interfacial roughness of the top and bottom electrodes which intensifies the electric field leading to lowering of the effective barrier height and hence increasing the current³¹.

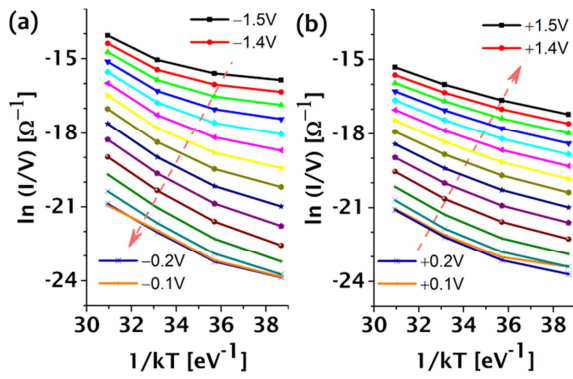


FIG. 5. Arrhenius plots of the *MIM* device S2 from 0 to +1.5 (a) and to -1.5 V (b) at a 0.1 V step voltage.

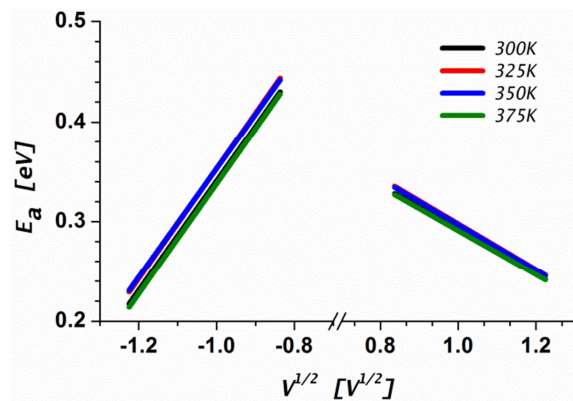


FIG. 6. Activation energy (E_a) versus square root of voltage plots for the *MIM* device S2 at 300, 325, 350, and 375 K.

B. Barrier tuning of double dielectric diodes

The effect of varying the individual layer thickness of Ta₂O₅ with a 1 nm thick Al₂O₃ dielectric can be observed in the rectifying characteristics shown in *FIG. 7*. It should be noted that the quantum well between the two dielectric layers becomes wider and deeper by either increasing the applied voltage or the thickness of the high- χ oxide (S6) giving rise to bound states in the quantum well³². The abrupt increase in the *J-V* plots (*FIG. 7.a*) at positive bias of 0.32 V for the 4 nm thick Ta₂O₅ oxide could be attributed to *RT*. This possibility is supported by the band diagrams of *FIG. 1.b* which indicate the probable occurrence of *RT* at positive bias, when the energy of a bound state in the well is matched to the states neighboring the Fermi level of the top Al charge injecting electrode³³. This provides further evidence that the noticeable improvement in asymmetry (*FIG. 7.b*) and non-linearity (*FIG. 7.c*) for S6 is associated with *RT*.

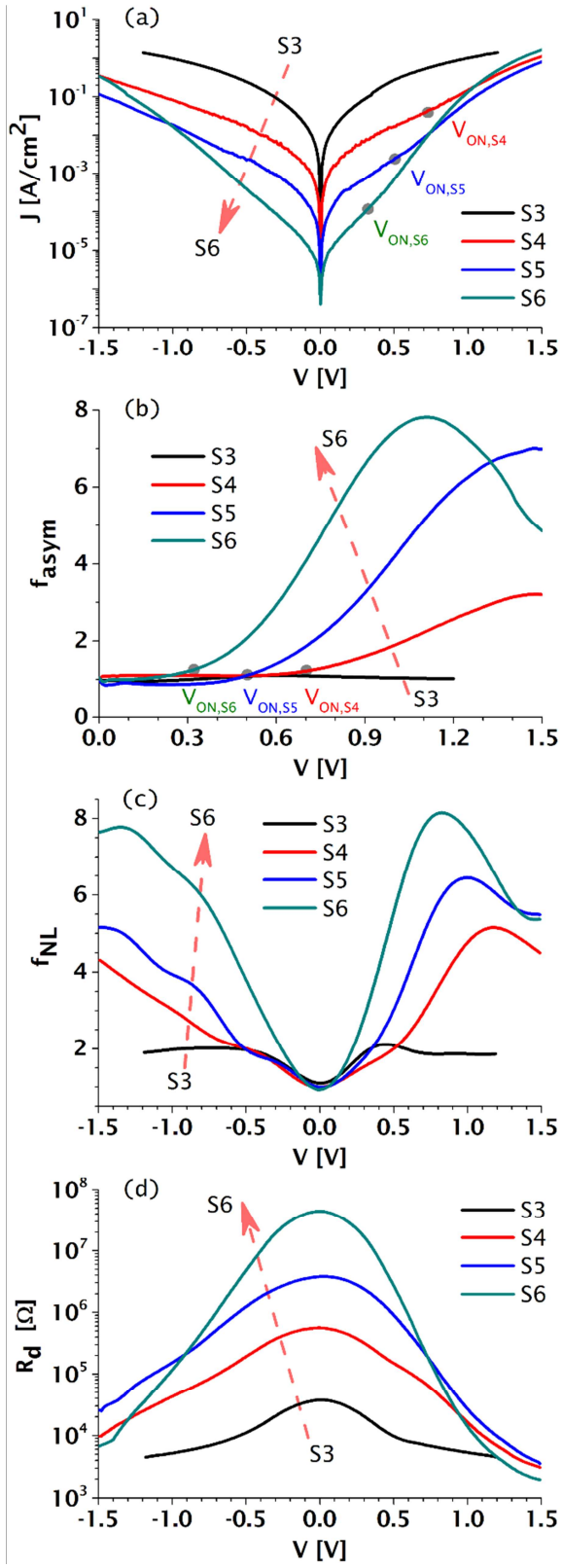


FIG. 7. The rectifying characteristics of the *MIIM* devices (S3, S4, S5, and S6) showing the: (a) J - V characteristics, (b) asymmetry, (c) non-linearity, and (d) dynamic resistance.

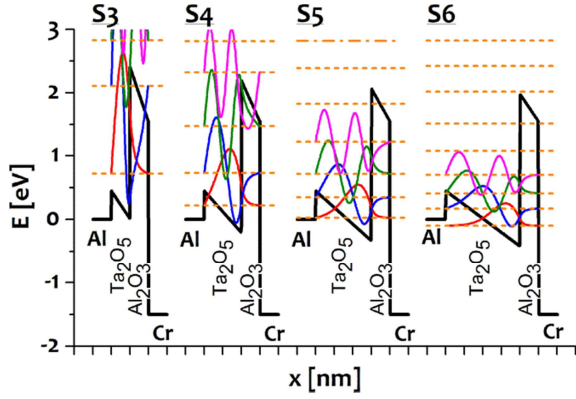


FIG. 8. Simulated conduction band diagrams at +1.5 V showing 0, 1, 2, and 3 bound states (dashed lines) for S3, S4, S5, and S6 respectively using a work function difference of 0.2 eV¹⁶.

Sample S3 shows inadequate non-linearity and asymmetry because the width of the quantum well in the device with 1 nm thick Ta₂O₅ is insufficient to accommodate a bound state in the range of the applied voltage (*FIG. 1.b*). *FIG. 8* shows the simulated conduction band diagrams, the wave function inside the dielectrics (sinusoidal waves), and the bound states for S3-S6 structures using an in-house model^{32,34}. The first bound state is predicted to be formed at an applied voltage of 0.89, 0.54, and 0.42 V for S4, S5, and S6 respectively. Briefly, we use the tunneling current equations and Tsu-Esaki method³⁵ to calculate the bound states in the quantum well within the conduction band of Ta₂O₅. We calculate the transmission probability by the transfer matrix method (TMA) that is, solving the time independent Schrödinger equation for each slice of the Tsu-Esaki multi-barrier oxide. The transmission probability is then integrated in the energy domain,

applying the Fermi-Dirac statistics for occupancy of electrons in the metal contacts, to calculate the current density.

In order to observe resonant tunneling, the quantum well (*FIG. 8*) needs to be sufficiently wide and deep to accommodate at least one bound state. The model does not take into consideration the charge trapping predicted from the domination of *PFE* in the high- κ Ta₂O₅ of defect nature. Other possibilities to explain the abrupt rise in the *J-V* characteristics are stress-induced leakage current (SILC)³⁶ and soft breakdown (SBD)³⁷. However, as no such rise in current could be observed for the *MIM* structures (S1-S2), these mechanisms are unlikely to explain that observed for the *MIIM* structures (S3-S6) fabricated at similar conditions.

A voltage V_{ON} is defined as the point at which the current abruptly increases or at the knee in the asymmetry plots. For S4, S5, and S6, V_{ON} is found to be 0.71, 0.5, and 0.32 V at positive bias in reasonable agreement with the theoretical prediction of the formation of a bound state. The decrease in V_{ON} with Ta₂O₅ thickness is consistent with the associated increase in the depth of the quantum well at positive bias as illustrated in *FIG. 8*. The larger current observed at positive bias for S4, S5, and S6 indicates that the overall asymmetry is regulated by the dominance of *RT* at positive bias over other conduction mechanisms. The effect of resonant tunneling is enhanced in structure S6 with a quantum well accommodating a number of bound states, at a certain voltage, larger than that in other *MIIM* structures (*FIG. 8*). For this device, the increase in non-linearity (*FIG. 7.c*) and the drop in dynamic resistance (*FIG. 7.d*) were steeper at positive bias, where *RT* occurs (*FIG. 1.b*), than at negative bias, where step tunneling occurs (*FIG. 1.a*), indicating the advantage of the prior mechanism in rectification. As the Ta₂O₅ thickness

is varied, a trade-off is apparent between the asymmetry, non-linearity, and low V_{ON} and the dynamic resistance (*FIG. 7.d*), which needs to be reduced for impedance matching in the THz rectenna. Accordingly, the choice of an optimum *RT* structure should take into consideration this trade-off depending on the application.

V. SUMMARY AND CONCLUSIONS

Atomic layer deposited Ta_2O_5 and Al_2O_3 oxides were used in single and double barrier structures to identify and optimize their rectifying performance. The dominant conduction mechanisms in 4 nm thick layers of Al_2O_3 and Ta_2O_5 were shown to be tunneling in the former and *PFE* in the latter. There was self-consistent evidence for resonant tunneling in double dielectric diodes arising from the noticeable enhancement in non-linearity and asymmetry in agreement with the theoretical modelling. The effect of *RT* was tuned according to the individual thickness of the Ta_2O_5 layer resulting in a noticeable improvement in rectification as the quantum well becomes wider such as to accommodate more bound states. Enhanced rectifying characteristics were observed at a turn-on voltage as low as 0.32 V. It is feasible that exploitation of work function engineering can further reduce the turn-on voltage to allow the zero-bias rectification³⁴ necessary for energy harvesting in rectenna structures.

ACKNOWLEDGMENTS

This work has been partly funded by EPSRC, UK, under project EP/K018930/1. The authors thank the collaborating partners: Dr J. Wrench and Prof P.R. Chalker from the Centre for Materials and Structures for the ALD. INN acknowledges the University of Liverpool and National Tsing Hua University for provision of a studentship.

- ¹ S. Hall, I. Z. Mitrovic, N. Sedghi, Y. C. Shen, Y. Huang, and J. F. Ralph, in *Functional Nanomaterials and Devices for Electronics, Sensors and Energy Harvesting*, edited by A. Nazarov et al. (Springer International Publishing, Switzerland, 2014), pp. 241.
- ² E. H. Hauge and J. A. Støvneng, *Reviews of Modern Physics* 61 (4), 917 (1989).
- ³ G. M. Elchinger, A. Sanchez, C. F. Davis, and A. Javan, *Journal of Applied Physics* 47 (2), 591 (1976).
- ⁴ M. Sarehraz, PhD thesis, University of South Florida, 2005.
- ⁵ P. C. D. Hobbs, F. R. Libsch, N. C. LaBianca, R. B. Laibowitz, and P. P. Chiniwalla, *Optics Express* 15 (25), 16376 (2007).
- ⁶ S. Grover, O. Dmitriyeva, G. Moddel, and M. J. Estes, *IEEE Transactions on Nanotechnology* 9 (6), 716 (2010).
- ⁷ M. Dagenais, K. Choi, F. Yesilkoy, A. N. Chryssis, and M. C. Peckerar, in *Optoelectronic Integrated Circuits XII* (Society of Photo-optical Instrumentation Engineers, 2010), Vol. 7605, pp. 76050E.
- ⁸ S. Bhansali, S. Krishnan, E. Stefanakos, and D. Y. Goswami, in *AIP Conference Proceedings* (American Institute of Physics, 2010), Vol. 1313, pp. 79.
- ⁹ Y. Huang and S. Hall and Y. Shen, UK Patent No. 2484526 (A) (2012).
- ¹⁰ G. Moddel and S. Grover, *Rectenna solar cells*. (Springer, New York, 2013).
- ¹¹ S. Grover and G. Moddel, *Solid State Electronics* 67 (1), 94 (2012).
- ¹² M. Feiginov, K. Hidetoshi, S. Safumi, and A. Masahiro, *Applied Physics Letters* 104 (24), 243509 (2014).
- ¹³ T. C. L. G. Sollner, W. D. Goodhue, P. E. Tannenwald, C. D. Parker, and D. D. Peck, *Applied Physics Letters* 43 (6), 588 (1983).
- ¹⁴ P. Maraghechi, A. Foroughi-Abari, K. Cadien, and A. Y. Elezzabi, *Applied Physics Letters* 100 (11), 113503 (2012).
- ¹⁵ B. Berland, NREL Subcontractor Final Report, ITN Energy Systems, Inc., Littleton Report No. NREL/SR-520-33263, 2003.
- ¹⁶ C. J. Smithells, W. F. Gale, and T. C. Totemeier, *Smithells Metals Reference Book*, 8th ed. (Elsevier Butterworth-Heinemann, Amsterdam, 2004), pp.18.
- ¹⁷ S. M. Sze and K. K. Ng, *Physics of semiconductor devices*, 3rd ed. (Wiley-Interscience, Hoboken, N.J., 2007), p.137.
- ¹⁸ R. G. Southwick, A. Sup, A. Jain, and W. B. Knowlton, *IEEE Transactions on Device and Materials Reliability* 11 (2), 236 (2011).
- ¹⁹ D. A. Buchanan, E. P. Gusev, E. Cartier, H. Okorn-Schmidt, K. Rim, M. A. Gribelyuk, A. Mocuta, A. Ajmera, M. Copel, S. Guha, N. Bojarczuk, A. Callegari, C. D'Emic, P. Kozlowski, K. Chan, R. J. Fleming, P. C. Jamison, J. Brown, and R. Arndt, *International Electron Devices Meeting 2000, Technical Digest*, 223 (2000).
- ²⁰ K. Kukli, M. Ritala, and M. Leskela, *Journal of the Electrochemical Society* 142 (5), 1670 (1995).
- ²¹ R. H. Fowler and L. Nordheim, in *Proceedings of the Royal Society of London* (The Royal Society, 1928), Vol. 119, pp. 173.
- ²² Y. Matsumoto, T. Hanajiri, T. Sugano, and T. Toyabe, *Japanese Journal of Applied Physics, Part 1: Regular Papers and Short Notes and Review Papers* 35 (2 Suppl. B), 1126 (1996).

- ²³ N. Sedghi, J. F. Ralph, I. Z. Mitrovic, S. Hall, and P. R. Chalker, *Applied Physics Letters* 102 (9), 092103 (2013).
- ²⁴ R. Winston Revie and Herbert Henry Uhlig, *Corrosion and corrosion control : an introduction to corrosion science and engineering*, 4th ed. (Wiley-Interscience, Hoboken, N.J., 2008), p.383.
- ²⁵ N. Alimardani, S. W. King, B. L. French, T. Cheng, B. P. Lampert, and J. F. Conley Jr, *Journal of Applied Physics* 116 (2), 024508 (2014).
- ²⁶ S. M. Sze, *Physics of semiconductor devices*. (Wiley-Interscience, 1969), p.496.
- ²⁷ W. R. Harrell and J. Frey, *Thin Solid Films* 352 (1–2), 195 (1999).
- ²⁸ A. G. Milnes, in *Deep impurities in semiconductors* (Wiley-Interscience, New York, 1973), pp. 99.
- ²⁹ R. A Ongaro and A. A Pillonnet, *Revue de Physique Appliquée* 24 (12), 1085 (1989).
- ³⁰ N. Alimardani, J. M. McGlone, J. F. Wager, and J. F. Conley, *Journal of Vacuum Science & Technology A* 32 (1), 01A122-1 (2013).
- ³¹ C. W. Miller, Z. P. Li, I. K. Schuller, and J. Åkerman, *Applied Physics Letters* 90 (4), 043513 (2007).
- ³² Z. Wang, J. Ralph, N. Sedghi, I. Z. Mitrovic, and S. Hall, *Journal of Vacuum Science & Technology B* 31 (2), 021209 (2013).
- ³³ L. L. Chang, L. Esaki, and R. Tsu, *Applied Physics Letters* 24 (12), 593 (1974).
- ³⁴ N. Sedghi, I. Z. Mitrovic, J. F. Ralph, and S. Hall, in *18th Workshop on Dielectrics in Microelectronics* (WODIM 2014, Cork, Ireland, 2014).
- ³⁵ R. Tsu and L. Esaki, *Applied Physics Letters* 22 (11), 562 (1973).
- ³⁶ E. Rosenbaum and L. F. Register, *Ieee Transactions on Electron Devices* 44 (2), 317 (1997).
- ³⁷ M. Depas, T. Nigam, and M. M. Heyns, *Ieee Transactions on Electron Devices* 43 (9), 1499 (1996).